ACS OMEGA

http://pubs.acs.org/journal/acsodf

Article

Improving the Electrochemical Properties of Carbon Paper as Cathodes for Microfluidic Fuel Cells by the Electrochemical Activation in Different Solutions

Chunmei Liu,* Canxing Sun, Yanjun Gao, Weijuan Lan, and Shaowei Chen*

Cite This: *ACS Omega* 2021, 6, 19153−19161

Read Online

ACCESS | Metrics & More | Article Recommendations | Supporting Information

ABSTRACT: Membraneless microfluidic fuel cells (MFCs) have garnered tremendous interest as micropower devices, which exploit the colaminar nature of two aqueous electrolytes to separate the anode and cathode and avoid the membrane usually used in a fuel cell. Our previous research shows that the performance of $FeCl_3$-based MFCs with catalyst-free cathodes is mainly limited by the cathode. To improve the power output of these MFCs, we activated the carbon paper cathode by an electrochemical method in the three solutions (Na_2SO_4, NaOH, and H_2SO_4) to improve the electrochemical characteristics of the carbon paper cathode. The surface functionalities and defects, reduction activation of iron ions as the oxidant, cathode resistance, and performance of $FeCl_3$-based MFCs were measured and compared. Our work shows that the electrochemical activation of the carbon paper in different solutions is a simple and effective method to enhance the electrochemical characteristics of the carbon paper cathode and improve the performance of the $FeCl_3$-based MFC. Also, the MFC with the carbon paper cathode activated in the H_2SO_4 solution reaches the optimum performance: 235.6 mW cm^{-3} in volumetric power density and 1063.33 mA cm^{-3} in volumetric limiting current density, which are 1.58 and 1.52 times as much as that of a MFC with an untreated carbon paper cathode, respectively. This best performance can be attributed to the cathode activated in the H_2SO_4 solution with the largest number of oxygen-containing functional groups, the largest electrochemical active surface area, strongest reduction of iron ions, and least resistance of the cathode.

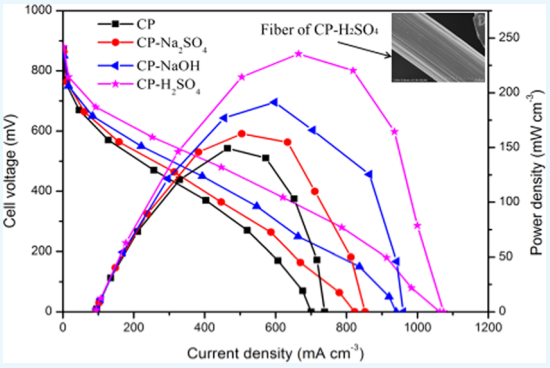

1. INTRODUCTION

Microfluidic fuel cell (MFC) is regarded as the next-generation micropower generator for portable electronics.[1] MFCs utilize the unique feature of co-flowing of two fluids in the microchannel, and the liquid−liquid interface serves as the separator, usually used in the conventional fuel cells.[2] These membraneless structures of MFCs not only reduce the cost and simplify the cell design but also eliminate the problems caused by the membrane, such as water management, membrane degeneration, and fuel crossover.[2,3]

Electrode materials are critical for the performance of MFCs as the sites of electrochemical reactions, the access of reactant delivery, and the media of electron collection. However, carbon fiber materials as electrodes endow some intrinsic weaknesses such as insufficient oxygen-containing groups on the surface and inadequate accessible surface areas, which result in the inferior physical and electrochemical characteristics of the electrodes themselves.[4] To improve the physical and electrochemical characteristics of the carbon fiber materials, various activation methods, including heteroatom doping,[5,6] surface functionalization,[7,8] defects and edge tailoring,[9] and porous structure and morphology engineering,[10,11] have been reported. Activated carbon electrodes have been applied in many fields and reported in several reviews as electrocatalysts for the oxygen reduction reaction (ORR), oxygen evolution reaction (OER), and hydrogen evolution reaction (HER)[12] and aqueous flow batteries[13] and electrochemical storage.[14] The electrochemical activation, as a simple and effective method, also has been widely applied to treat commercial carbon fiber materials.[14,15] It has been reported that acids (HNO_3, H_2SO_4/HNO_3 mixture, and H_3PO_4),[16−18] alkali (NaOH and KOH),[19,20] water-soluble salts (Na_2SO_4, K_2CO_3), and other reagents[21,22] are used as electrolytes for electrochemical modifications.

In MFCs, many oxidants have been studied, such as air,[23,24] H_2O_2,[25] ClO^-,[26] $KMnO_4$,[27] VO_2^+,[28] and Fe^{3+}.[29,30] These oxidants of O_2, H_2O_2, ClO^-, and $Cr_2O_7^-$ require noble or nonnoble metals as catalysts to obtain better oxidability. Some oxidants of $KMnO_4$ and VO_2^+ do not need a catalyst but have

Received: May 12, 2021
Accepted: June 30, 2021
Published: July 15, 2021

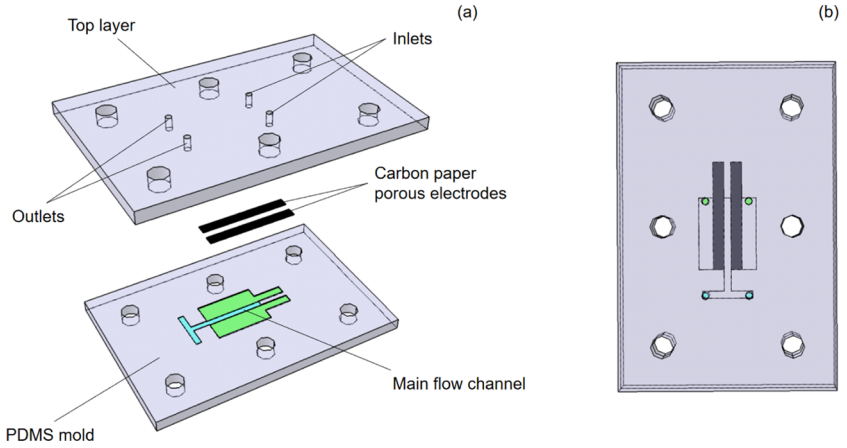

Figure 1. Schematic figure of the MFC using the flow-through carbon paper electrode ((a) explosive view of the MFC design and (b) top view of the lower plate of the MFC).

their own disadvantages when used in MFCs. The reduction product of $KMnO_4$ is MnO_2 granules, which can attach onto the electrode surface and block the transport of the oxidant to the electrode. VO_2^+ with its toxicity can pollute soil and water resources. Also, it is reported that the exchange current density of the iron redox pair (10^{-2} A cm^{-2}) is several orders of magnitude higher than that of the oxygen gas (10^{-10} A cm^{-2}).[31] The adoption of iron chloride as the oxidant in MFCs has distinct advantages of safety, environmental friendliness, and operation without the need for cathode catalysts. Our previous study shows that the performance of $FeCl_3$-based MFCs is mainly limited by the cathode. Carbon fiber paper has been widely used as the electrodes of MFCs. Thus, it is indispensable to activate the carbon paper adopted as cathode electrodes of the MFCs. The commercial carbon paper by a simple electrochemical activation in different solutions as cathode materials of MFCs has not been studied thoroughly.

In this work, we first performed the activation of the carbon paper electrode by the electrochemical methods in three different fluids: (1) the neutral solution (Na_2SO_4 solution), (2) the alkali solution (NaOH solution), and (3) the acidic solution (H_2SO_4 solution). Three activated carbon paper electrodes were adopted as the cathode materials of a MFC with formic acid (HCOOH) as a fuel and iron chloride ($FeCl_3$) as an oxidant. Then, the diversified physical characterizations of the varied cathode electrodes were investigated to gain the surface morphologies, functional groups, surface defects, and hydrophilicity of the various cathode electrodes. Meanwhile, detailed electrochemical experiments such as cyclic voltammogram (CV) and electrochemical impedance spectroscopy (EIS) measurements were performed to obtain the reduction activity of Fe^{3+} ions and cathode resistance, respectively. Finally, the performances of the MFC with the three groups of cathodes were compared, and the performance of the MFC with the carbon paper activated in the H_2SO_4 solution was found to be optimum. From the physical and electrochemical results, we can attribute the best performance to the advantages of the abundant oxygen-containing functionalities, surface defects on the carbon fibers, electrochemically active surface area (EASA), and cathode resistance.

2. EXPERIMENTAL SECTION

2.1. Electrode Materials. The anode and cathode electrodes used in the experiment were both carbon paper (HCP020N; Shanghai Hesen Electric Co. Ltd., China). The size of each electrode was about 200 μm (thick) × 1.5 mm (wide) × 15 mm (long). In consideration of the overlap between the electrode clamp and electrode, the exposed electrode size of the anode for the electrodeposition and cathode for the electrochemical activation was 200 μm (thick) × 1.5 mm (wide) × 10 mm (long).

As the cathode electrode, the carbon paper was activated by the identical current density (30 mA cm^{-2}) and the same treatment time (30 min) at ambient temperature in the different solutions. The treatment experiment was accomplished by the electrochemical workstation (ZENNIUM, Germany) in a three-electrode measurement mode. The CP, CP-Na_2SO_4, CP-NaOH, and CP-H_2SO_4 electrodes were used to represent the carbon paper electrode without any treatment and the carbon paper activated in 0.5 mol L^{-1} Na_2SO_4 (pH = 6.8), 1 mol L^{-1} NaOH (pH = 14), and 0.5 mol L^{-1} H_2SO_4 (pH = 0) solution, respectively. The pHs of the solutions were measured by FE20 pH meter (Mettler Toledo). After treatment, the carbon paper electrodes were washed with plenty of deionized water until the solution on the surface of the carbon paper was neutral (pH ∼ 7). Finally, the carbon paper electrodes were dried at 60 °C in a drying oven for 24 h before use.

As the anode electrode, the untreated carbon paper was loaded with palladium nanoparticles as the catalysts. The electrodeposition was also conducted by the electrochemical workstation in a three-electrode system. The palladium catalyst was electrodeposited at 0 V vs Ag/AgCl (in saturated KCl, 0.198 V) until the palladium catalyst loading was 5 mg cm^{-2} under the assumption that the Coulombic efficiency was 60%.[32,33] The detailed surface morphologies and crystal size of the anode palladium catalysts can be found in our previous research.[29,30]

2.2. Electrode Characterizations. The Hitachi field emission scanning electron microscope (FESEM; SU8020, Japan) was employed to observe the surface morphologies for the carbon fibers of the four samples. To gain distinct images, a thin gold film was sprayed on the surface of each sample before the observation.

The Nicolet Fourier transformed infrared spectroscopy (FTIR; Nexus 410, GMI Inc.) was adopted to determine the functional groups on the surfaces of the four samples. Before the FTIR test, each cathode paper was crushed into powder

https://doi.org/10.1021/acsomega.1c02507
ACS Omega 2021, 6, 19153−19161

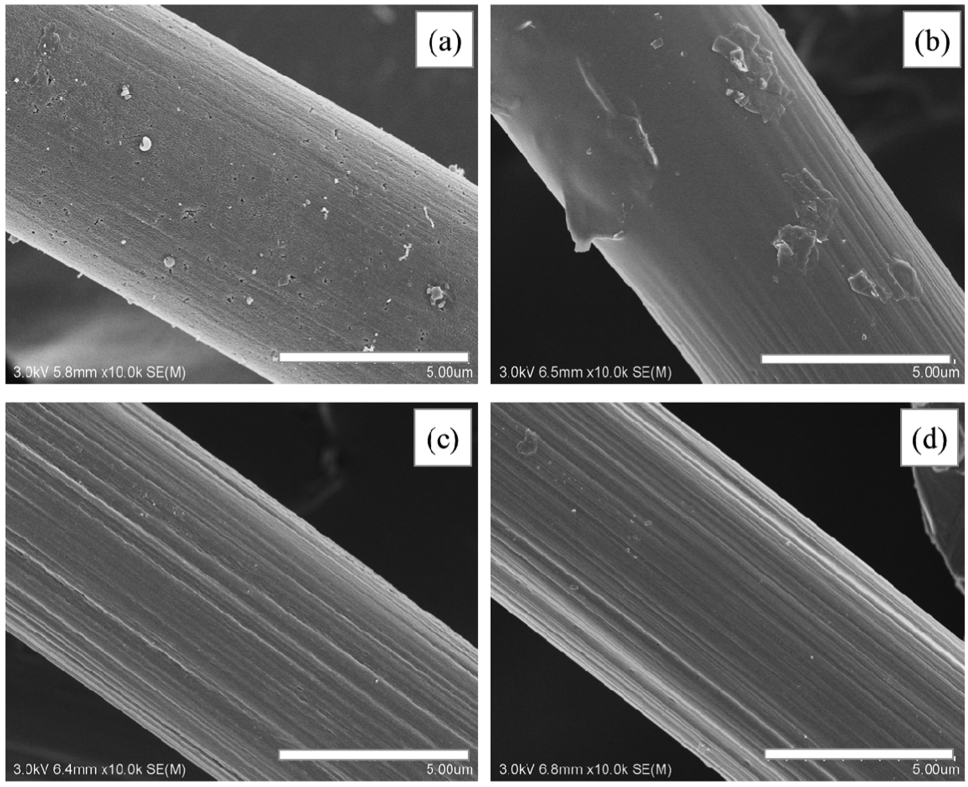

Figure 2. FESEM figures of carbon fibers of the four cathodes with 10000× magnification: (a) CP, (b) CP-Na_2SO_4, (c) CP-NaOH, and (d) CP-H_2SO_4. Scale bar: 5 μm.

form, respectively. Then, about 0.5 mg carbon and 40 mg potassium bromide powders were fully mixed, and the mixed powder was squeezed into a disk to conduct the FTIR measurement. The FTIR spectrum curves were obtained by the accumulation of 32 scans with a 2 cm^{-1} spectral resolution.

Thermo X-ray photoelectron spectroscopy (XPS; ESCALAB 250XI) was used to determine the composition on the surfaces of the four samples with an Al Kα radiation source (1486.6 eV). *Xpspeak* 4.1 software was adopted to analyze the XPS spectra.

The Raman spectrometer (Renishaw inVia, U.K.) was employed to measure the degree of surface defect of the carbon paper with a 532 nm excitation wavelength.

The contact-angle goniometer (OCA50, Germany) was used to gain the surface hydrophilicity of the paper samples. During this measurement, the ultrapure water was carefully dropped onto the sample surface.

2.3. MFC Setup and Operations. The MFC was mainly comprised of the two poly(dimethylsiloxane) (PDMS) substrates. There were two 3 mm holes as the inlets and two 3 mm holes as the outlets in the upper plate. There existed three channels in the lower plate: the one in the middle of the plate as the main flow channel and the other two as the electrode channels. Before the assembly of the MFC, the cathode and anode electrodes were carefully placed in the electrode channel, respectively. The titanium foil (0.25 mm in thickness) was adopted as the current collector, touching the front section (5 mm in length) of the electrodes to collect the electrons from/to the electrodes. Therefore, the actual working electrode size was ~200 μm in thickness, 1.5 mm in width, and 10 mm in length. Figure 1 shows the schematic figure of our MFC. The MFC assembly processes can be found in our previous report[29,30] and in the Supporting Information in detail.

The anolyte used in the experiment was composed of 1 M formic acid (the fuel) and 1 M sulfuric acid (the supporting electrolyte) solutions. The catholyte was made of 0.2 M $FeCl_3$ (the oxidant) and 1 M HCl (the supporting electrolyte) solutions. The anolyte and catholyte fluids were simultaneously injected by the LSP02-1B Longer syringe pump (Baoding, China) with the double channels to deliver into the inlets, through the electrodes and the main flow channel, and finally removed from the outlets to the waste liquid reservoir. During the whole experiment, the flow rates of the solutions were kept at 20 mL h^{-1}.

2.4. Electrochemical Measurements. All of the electrochemical experiments were accomplished by the ZENNIUM electrochemical workstation. The electrochemical measurements, mainly including the cyclic voltammogram (CV) and electrochemical impedance spectroscopy (EIS) measurements, were carried out in the three-electrode mode. The activated carbon paper served as the working electrode, and a Pt sheet (20 mm × 50 mm) and a saturated Ag/AgCl electrode (0.198 V vs standard hydrogen electrode (SHE)) were used as the counter electrode and the reference electrode, respectively. To investigate the reduction of the oxidant on the different cathode electrodes, CV experiments were carried out between 0.0 and 1.0 V vs Ag/AgCl at a scan rate of 10 mV s^{-1}. The EIS measurements were performed in a frequency range of 100 kHz and 100 mHz with an excitation signal of 5 mV under open-circuit potentials (OCPs). The CV and EIS experiments were all conducted in a catholyte made of 0.2 M $FeCl_3$ and 1 M HCl solution.

The polarization curves of the MFCs with the varied cathodes were obtained by the chronoamperometry method

https://doi.org/10.1021/acsomega.1c02507
ACS Omega 2021, 6, 19153−19161

with a series of potentiostatic operations from the OCP to 0.0 V with a decrease of 100 mV per operation. It was kept for 180 s at each cell voltage, while the currents at each steady voltage were recorded. At the same time, the cathode potentials were monitored and noted down, as values vs saturated Ag/AgCl reference electrode deposited at the catholyte outlet. The anode potentials were gained through cathode potentials minus the cell voltages. In the MFCs adopting the flow-through electrodes, there was some discrepancy in the area to gain the current and power density, whether the projected electrode area or the area cross-sectional to the reactant flow. To avoid ambiguity, we adopted the volumetric current density and power density based on the actual volume of the electrode (0.003 cm^3) to compare the performance of the MFCs.[29,30]

To obtain reliable experimental results, all experiments were performed at least three times and processed at a room temperature of about 293 K.

3. RESULTS AND DISCUSSION

3.1. Surface Morphologies by SEM. The surface morphologies of the carbon fibers from the four cathodes were seen in the FESEM images (Figure 2). All of the fibers showed the same diameter of about 7 μm. It could be obviously seen that all three treated carbon paper displayed much rougher surfaces with many deep ditches after the treatment, while the untreated carbon paper showed a smooth surface. This means that the electrochemical treatment of the carbon paper can etch the carbon fibers and also implies that the surfaces of the treated electrodes have been increased. In addition, it is worth noting that the CP-NaOH and CP-H_2SO_4 electrodes both demonstrated a much deeper and more thorough degree of etching compared with the CP-Na_2SO_4 electrode. This indicates that the effects of electrochemical treatment in an alkaline or acidic solution are better than that in a neutral solution.

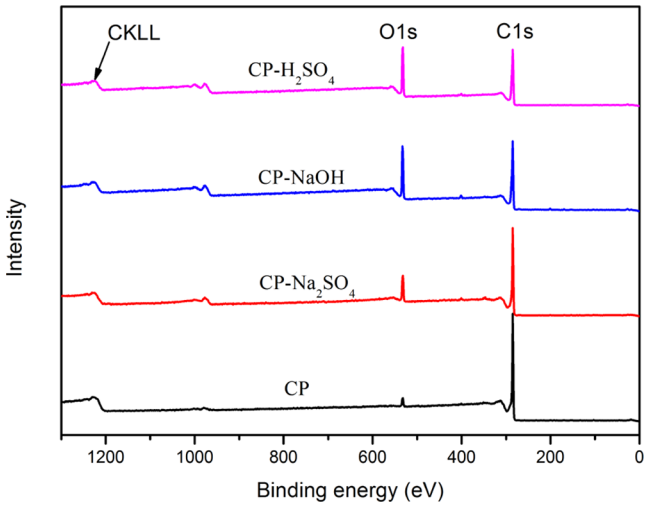

Figure 3. XPS spectrum curves of the four electrodes.

3.2. XPS Results. In the FTIR results (Figure S1, Supporting Information), all of the sample electrodes can be seen to display five vibrational peaks, suggesting that the types of the functional groups are the same for the four samples. To quantify the surface functional groups of the four electrodes, the XPS measurements were performed, as shown in Figure 3. As seen in Figure 3, all four samples show two distinct peaks: one stronger peak for C 1s at a binding energy of about 285 eV and the other strong peak for O 1s at about 533 eV. The binding energy of 284.8 eV of the major C 1s peak was taken as the reference to calibrate all spectra.

To obtain the individual contents of the surface functional groups, *Xpspeak* 4.1 program was used to deconvolve the two strong C 1s and O 1s peaks, as shown in Figure 4. Curve deconvolution was performed following a Shirley-type background subtraction with a Gaussian−Lorentzian function as the fitting method. The contents of each surface functional group for the four electrodes can be obtained from Figures 3 and 4 by calculating its relative peak area; the results are displayed in Table 1.

From Figure 4, the intensity of the main O 1s peak at ~533 eV increases, while that of the main C 1s peak at ~284.8 eV decreases according to the sequence: CP, CP-Na_2SO_4, CP-NaOH, and CP-H_2SO_4. This variation tendency indicates that the O element content and O/C ratio increase in accordance with the above sequence. It is verified from Table 1 that the O content of the CP-H_2SO_4 electrode reaches 15.80% from

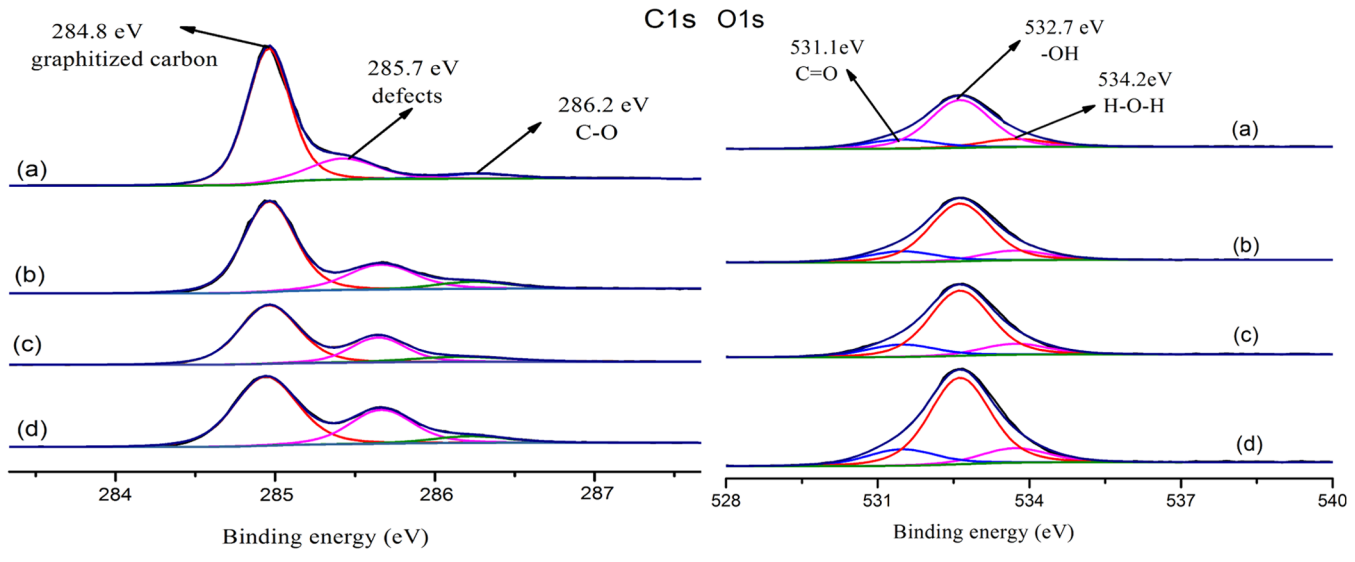

Figure 4. XPS analysis of C 1s and O 1s peaks for the four cathodes: (a) CP, (b) CP-Na_2SO_4, (c) CP-NaOH, and (d) CP-H_2SO_4.

https://doi.org/10.1021/acsomega.1c02507
ACS Omega 2021, 6, 19153−19161

Table 1. Contents of Surface Elements and Oxygen-Containing Groups on the Four Samples

samples	C content (x_{at} %)	graphitized carbon content (x_{at} %)	defects	O content (x_{at} %)	O/C ratio	O−H content (x_{at} %)	H−O−H content (x_{at} %)	C═O content (x_{at} %)
CP	91	70.12	16.78	8.67	0.12	6.19	1.13	1.34
CP-Na_2SO_4	89	60.48	21.89	11.30	0.19	7.91	1.63	1.76
CP-NaOH	86	55.75	22.21	13.40	0.24	9.68	1.85	1.87
CP-H_2SO_4	84	52.48	25.51	15.80	0.30	11.28	2.30	2.22

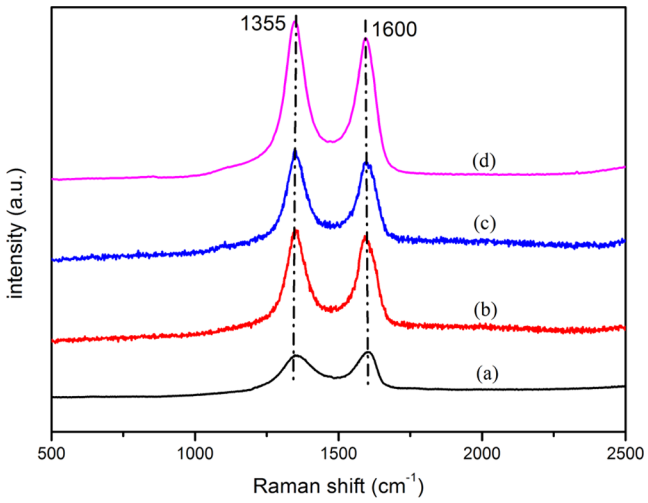

Figure 5. Raman spectra for the four carbon paper electrodes: (a) CP, (b) CP-Na_2SO_4, (c) CP-NaOH, and (d) CP-H_2SO_4.

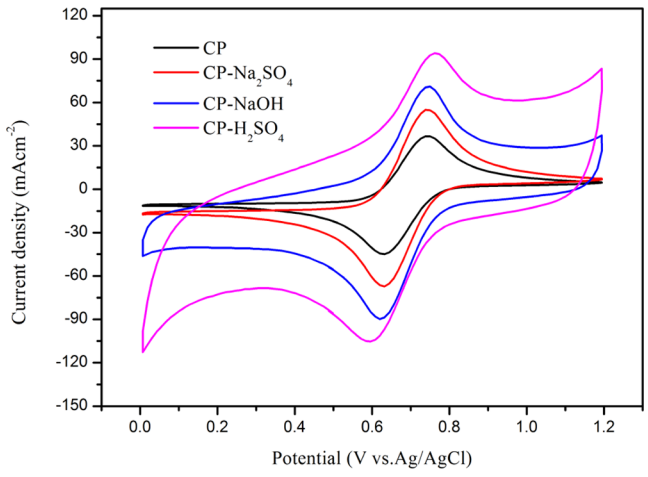

Figure 6. CV results for the four cathodes in the catholyte solution at a scan rate of 10 mV s^{-1}.

8.67% of the CP electrode after the activation. Correspondingly, the O/C ratio of the CP-H_2SO_4 electrode increases to 0.30 from 0.12 of the CP electrode. This reveals that the electrochemical activation of the carbon paper could introduce the functional groups on the carbon fiber surfaces.

As shown in Figure 4, the deconvolution of the C 1s spectra yielded three peaks. The three peaks can be attributed to the graphitized carbon of graphitic carbon (C═C) and the hydridized carbon (C−C) at ∼284.8 eV, surface defects on the carbon fibers at ∼285.7 eV,[34] and the carbon in the −OH groups (C−OH) at ∼286.2 eV.[35] The deconvolution of the C 1s spectra presents the decreased graphitized carbon content after the treatment. In addition to a decrease in the graphitized carbon content, the defect peak reveals an increase after treatment, which can be confirmed from the FESEM images.

Meanwhile, the deconvolution of the O 1s spectra produced three peaks: C═O (531.1 eV), −OH (532.7 eV), and H−O−H (534.2 eV, the adsorbed water molecules) functional groups.[36,37] Among these oxygen-containing groups, the

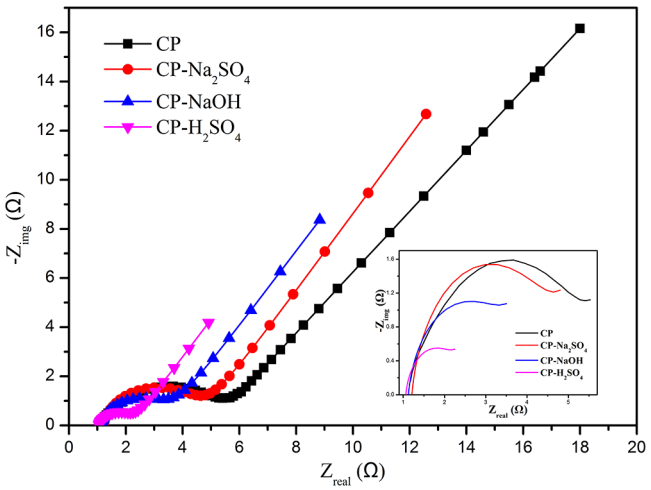

Figure 7. Nyquist plots of the different cathodes under the open-circuit potentials.

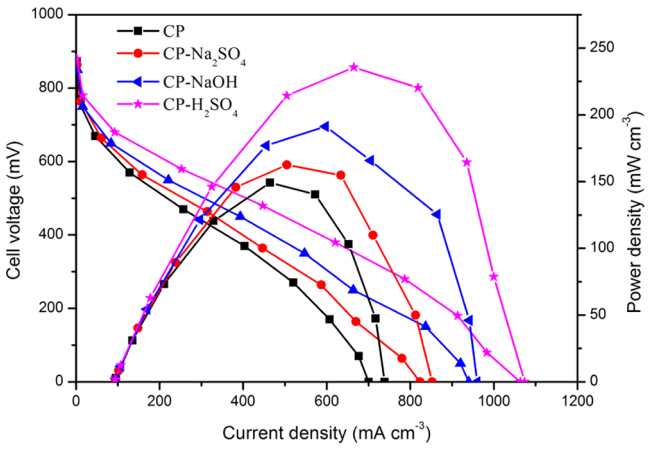

Figure 8. Power density plots and polarization plots of the MFCs with the different carbon paper cathodes.

Table 2. Cathode Resistances Estimated from the Nyquist Plots

cathode	R_s (Ω)	R_{ct} (Ω)	R_d (Ω)	R_t (Ω)
CP	1.1	4.8	4.8	10.7
CP-Na_2SO_4	1.1	4.1	4.0	9.2
CP-NaOH	1.1	3.2	3.2	7.59
CP-H_2SO_4	1.1	1.5	2.0	4.6

https://doi.org/10.1021/acsomega.1c02507
ACS Omega 2021, 6, 19153−19161

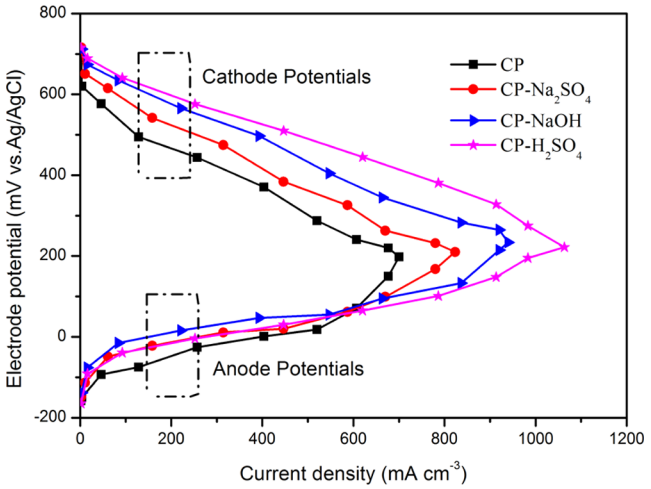

Figure 9. Electrode potentials of the MFCs with the different carbon paper cathodes.

Table 3. Limiting Current Densities and Maximum Power Densities of the MFCs with the Different Cathodes

cathode electrode	limiting current density (mA cm^{-3})	maximum power density (mW cm^{-3})
CP	700	149.23
CP-Na_2SO_4	823.33	162.59
CP-NaOH	940	191.33
CP-H_2SO_4	1063.33	235.6

−OH functional groups play a vital role in the electron transfer between the electrolyte and carbon materials as the active sites.[38,39] As seen in Table 1, the −OH group content occupies the largest proportion in the three functional groups and obviously increases from 6.19% in CP to 11.28% in CP-H_2SO_4. The C═O functional groups mainly stem from further oxidization of −OH groups when the fragments of C═C bonds are broken under the condition of strong oxidation.[37] The C═O group contents are as follows: 1.34% (CP), 1.76% (CP-Na_2SO_4), 1.87% (CP-NaOH), and 2.22% (CP-H_2SO_4). From the variation trend in the content of the −OH and C═O groups, it is concluded that the electrochemical activation in the H_2SO_4 solution can introduce the most oxygen-containing groups. Moreover, the change of the water content absorbed on the carbon fiber surfaces is in accordance with that of the −OH group content, displayed in Table 1. This means that surface polarity and hydrophility on the carbon fibers both can be improved by electrochemical activation. The hydrophilicity of the carbon fiber samples is verified by the contact angle measurements (Figure S2 for CP electrode, Videos S1, S2, and S3 for CP-Na_2SO_4, CP-NaOH, and CP-H_2SO_4, respectively, Supporting Information).

In a word, after the electrochemical activation, the treated carbon paper can introduce more number of functional groups containing oxygen elements, which can supply more active places and enhance the wettability of the carbon paper surface. These improvements benefit the diffusion of the oxidant solution. We speculate that the CP-H_2SO_4 electrode has the largest number of active sites as it has the largest number of oxygen-containing functionalities anchored on its surface among the four electrodes.

3.3. Raman Analysis. To study the surface structures of the carbon samples, Raman spectroscopy was adopted within the Raman shift of 500−2500 cm^{-1}, and the Raman spectra are presented in Figure 5. All samples showed two distinct peaks. The two distinct peaks at 1350 and 1600 cm^{-1} are corresponding to a disordered amorphous carbon (D band) and a graphitic carbon (G band), respectively.[40] The intensity ratios of the D band to G band (I_D/I_G) were adopted to estimate the surface defect degree of these four samples.[41] The values of I_D/I_G for the CP, CP-Na_2SO_4, CP-NaOH, and CP-H_2SO_4 electrodes were calculated to be 0.95, 1.06, 1.09, and 1.11, respectively. The larger values for the activated electrode suggest that these electrodes possess more disordered characteristics and defects on the surface compared with pristine CP, which correspond with the FESEM results.

3.4. CV Results. To estimate the accessible surface areas of the four different cathodes, the CV measurements in 0.1 M $LiClO_4$ + 5 mM $K_3[Fe(CN)_6]$ solution were carried out with varied scanning rates (Figure S4). By calculation, the quantitative EASAs for the CP, CP-Na_2SO_4, CP-NaOH, and CP-H_2SO_4 electrodes were 0.32, 0.35, 1.41, and 1.73 cm^2, respectively. It can be observed that the EASAs of all of the activated electrodes are higher than that of the CP electrode, suggesting that the treated electrodes could provide a more ion-accessible surface area and enhance the power density. The highest EASA of the CP-H_2SO_4 electrode indicates that the electrode possesses the most available surface area for the transportation of the reactant ions, thereby improving power output.

To study the redox electrochemical activity of Fe^{3+} ions on the various cathodes, the CV measurement experiments for the four different cathodes in catholyte solutions were performed. The CV plots of the CP, CP-Na_2SO_4, CP-NaOH, and CP-H_2SO_4 cathodes conducted in catholyte (0.2 M $FeCl_3$ + 1 M HCl solutions) are shown in Figure 6. The reduction peak current density of the CP-H_2SO_4, CP-NaOH, and CP-Na_2SO_4 cathodes were 112.6, 89.8, and 67.3 mA cm^{-2}, respectively, which was much larger than that of the CP cathode (44.9 mA cm^{-2}). The incremental currents undoubtedly testify that Fe^{3+} ions are prone to take the reduction reaction at the surface of the activated carbon paper electrodes. The improved reduction can be attributed to two aspects: the augmentation of EASA

Table 4. Characteristics and Performance Summary of Some MFCs

fuel/oxidant	cathode catalyst	electrode active volume (cm^3)	OCV (V)	I_{max} (mA)	P_{max} (mW)	reference
HCOOH/$FeCl_3$	none	0.003	0.88	1063.33	235.6	this work
HCOOH/$KMnO_4$	none	0.817	1.2	28.16	14.74	28
HCOOH/air	Pt	0.027	~0.9	924.6	160	23
HCOOH/air	Pd@graphene	0.00225	~0.7	1160	608	24
HCOONa/air	Pt	0.0054	~1.0	3821	749.33	52
HCOONa/ClO^-	Pd	0.0036	1.45	8000	1733	26
HCOOH/H_2O_2	Pt	0.0035	1.1	2142	428.6	25

https://doi.org/10.1021/acsomega.1c02507
ACS Omega 2021, 6, 19153−19161

and the amount of functional groups containing oxygen elements. The improved EASA significantly increases the accessible surface area to develop −OH and C═O groups that produce the inner sphere action from the interaction of the surface oxides and soluble iron ions to facilitate the electron transfer.[42] Significantly, the electron transfer rate of Fe^{3+} ions is susceptible to be influenced by the surface C═O groups and increases with the addition of the C═O groups.[43]

3.5. EIS Results. To investigate the cathode resistance with the different cathode electrodes, the EIS measurements were carried out at the open-circuit potentials in the catholyte (0.2 M $FeCl_3$ + 1 M HCl solutions). The Nyquist plots of the four cathodes obtained by the EIS electrochemical method are shown in Figure 7.

In Figure 7, all Nyquist plots of the four cathode electrodes consist of the semicircle part at the high frequencies and a linear part at the low frequencies. The semicircle arises from the charge transfer processes at the catholyte and cathode interface.[44] The linear part at the low frequencies can be ascribed to the Warburg diffusion resistance (R_d), representing the diffusion of the ions of the catholyte in/out the interspaces of cathodes.[45,46] These results suggest that the reduction of Fe^{3+} ions on the surfaces of the cathodes is manipulated both by the charge transferring and diffusion processes.

The radius magnitude of the semiarc can be used to evaluate the resistance of charge transfer reaction (R_{ct}).[47] In Figure 8, the CP electrode has the biggest semiarc radius, suggesting that the CP electrode has the largest R_{ct} for the reduction reaction of the Fe^{3+} ions. In addition, the estimated R_{ct} values decrease according to the sequence CP, CP-Na_2SO_4, CP-NaOH, and CP-H_2SO_4. These results show that the electrochemical oxidation of the carbon paper electrode can effectually lower the R_{ct} for the reduction of Fe^{3+} ions; the R_{ct} for the CP-H_2SO_4 electrode was the least (∼1.5 Ω), while the R_{ct} for the CP electrode was the largest (∼4.8 Ω).

R_d could be evaluated from the intersection between the linear part and the horizontal axis at the low frequency.[48] The magnitude of the R_d for the CP, CP-Na_2SO_4, CP-NaOH, and CP-H_2SO_4 electrodes are evaluated as 4.8, 4.0, 3.2, and 2.0 Ω, respectively.

The R_{ct} and R_d values of the four electrodes decrease obviously according to the order CP, CP-Na_2SO_4, CP-NaOH, and CP-H_2SO_4 owing to the increase in the EASA and functional groups containing oxygen element on the electrode after activation. Especially, the existence of C═O functional groups enhances the redox reaction of Fe^{3+} ions and thus reduces the R_{ct}. The large EASA can not only provide a large accessible area to facilitate the reduction of Fe^{3+} ions but also benefit the diffusion processes of the ions between the catholyte and the CP-H_2SO_4 electrode.

The ohmic resistance (R_s) can be estimated from the intersection of the Nyquist plots with the horizontal axis at the high frequency.[44,46] R_s consists of the cathode electrode resistance, catholyte resistance, and contact resistance from the cathode and the current collector. From Figure 7, R_s for the four electrodes can be estimated to be about 1.1 Ω. The inconspicuous variation in R_s shows that our activations do not distinctly decrease the conductivity of the carbon paper electrode.

The estimated three resistances (R_{ct}, R_d, and R_s) are listed in Table 2; the total resistance (R_t) of the cathode electrode can be obtained as the sum of R_{ct}, R_d, and R_s. In Figure 8 and Table 2, the R_t of the CP-H_2SO_4 electrode is the least, suggesting that the cathode resistance of the CP electrode by electrochemical treatment is largely reduced and the effect of activation in the acidic solution is best.

3.6. MFC Performance. To compare the MFC performance with the four cathode electrodes, the MFCs with the CP, CP-Na_2SO_4, CP-NaOH, and CP-H_2SO_4 cathodes, and anode electrodes with the identical palladium catalyst loading were constructed. The MFC performance curves and electrode potentials plots are displayed in Figures 8 and 9, respectively, and the maximum power densities and largest current densities (limiting current densities) for these four assembled MFCs are demonstrated in Table 3.

Among these MFCs, the one with the CP-H_2SO_4 cathode shows the largest volumetric peak power density and the highest volumetric limiting current density of 235.6 mW cm^{-3} and 1063.33 mA cm^{-3}, respectively. The peak power density with the CP-H_2SO_4 cathode is about 1.58, 1.45, and 1.23 times as much as that of the MFCs with the CP cathode, the CP-Na_2SO_4 cathode, and the CP-NaOH cathode, respectively. From the figure (Figure 9) of the electrode potentials, it is concluded that the difference in the performance of the MFCs mainly arises from the carbon paper cathodes: the CP-H_2SO_4 electrode always exhibits the largest cathode potentials at the varied current densities.

From the above discussion, the MFC with the CP-H_2SO_4 cathode shows the optimum performance due to the largest number of functional groups containing oxygen elements, the highest EASA, and the least resistance of the cathode.

The comparisons of MFC performance between our work and that of others are shown in Table 4. In Table 4, although the peak power density and maximum current density of our MFC are not the largest, our MFC with iron ions as the oxidants have some obvious advantages with environmental friendliness, operation obviating the need for cathode catalyst, and good solubility of itself and its reduction products. The theoretical potential of Fe^{3+} is much lower than that of other liquid oxidants (H_2O_2, $KMnO_4$, ClO^-),[49] so the OCV of our MFC is almost the lowest in Table 4. The higher performance of $FeCl_3$-based MFCs could be obtained by adding some chelate compounds in the catholyte to enlarge the thermodynamic equilibrium potential range of Fe^{3+} ions.[50,51]

4. CONCLUSIONS

In this research, we adopted the electrochemical method in the different solutions (neutral, alkaline, and acidic solutions) to activate the carbon paper electrodes, which are usually used as the flow-through electrodes in the MFCs. We have investigated the surface morphologies, functional groups, degree of surface defects, EASAs, reduction of Fe^{3+} ions, and resistances of the carbon paper activated in the three different solutions: the neutral, alkaline, and acidic solution. Physical characterizations on the carbon paper surface on the four cathodes by FTIR, XPS, and Raman measurements revealed that the CP-H_2SO_4 electrode had the largest number of hydroxyl and carbonyl functional groups on its surface. CV and EIS electrochemical experiments revealed that the CP-H_2SO_4 electrode had the largest EASA; the Fe^{3+}/Fe^{2+} redox couple exhibited the strongest reduction and the least resistance of the cathode. With the combination of these advantages of the CP-H_2SO_4 electrode, the performance of the $FeCl_3$-based MFC with the CP-H_2SO_4 cathode was optimum among all of the MFCs with the activated cathodes. The maximum power density and limiting current density were largest with values of 235.6 mW

https://doi.org/10.1021/acsomega.1c02507
ACS Omega 2021, 6, 19153−19161

cm^{-3} and 1063.33 mA cm^{-3}, respectively, which were 1.58 and 1.52 times as much as that of a MFC with the CP cathode electrode, respectively.

This work also reveals that it is more effective to obtain better performance of the MFCs with the carbon paper cathode modified in the acidic solution by the electrochemical activation. Our results are anticipated to be practicable to other carbon-based electrodes but the activation conditions, e.g., solution concentrations, current density, and treatment duration time, might be carefully regulated on a case-by-case basis as regards the varied electrode materials.

■ ASSOCIATED CONTENT

Supporting Information

The Supporting Information is available free of charge at https://pubs.acs.org/doi/10.1021/acsomega.1c02507.

Contact-angle experiment for the CP-Na_2SO_4 electrode (Video S1) (AVI)

Contact-angle experiment for the CP-NaOH electrode (Video S2) (AVI)

Contact-angle experiment for the CP-H_2SO_4 electrode (Video S3) (AVI)

Detailed assembly processes of our MFC; FTIR results for the four cathode samples (Figure S1); contact angle measurement results for the four cathodes (Figure S2); electrochemically active surface areas (EASAs) of the four carbon paper cathodes by CV experiments at the different scans (Figure S3); and details of how to calculate the active electrode volume in Table 4 (PDF)

■ AUTHOR INFORMATION

Corresponding Authors

Chunmei Liu − *Institute of Vehicle and Transportation Engineering, Henan University of Science and Technology, Luoyang 471003 Henan, China;* orcid.org/0000-0003-0877-1427; Email: liuchm800226@163.com

Shaowei Chen − *Department of Chemistry and Biochemistry, University of California, Santa Cruz, California 95064, United States;* orcid.org/0000-0002-3668-8551; Email: shaowei@ucsc.edu

Authors

Canxing Sun − *Institute of Vehicle and Transportation Engineering, Henan University of Science and Technology, Luoyang 471003 Henan, China*

Yanjun Gao − *Institute of Vehicle and Transportation Engineering, Henan University of Science and Technology, Luoyang 471003 Henan, China*

Weijuan Lan − *Institute of Vehicle and Transportation Engineering, Henan University of Science and Technology, Luoyang 471003 Henan, China*

Complete contact information is available at: https://pubs.acs.org/10.1021/acsomega.1c02507

Notes

The authors declare no competing financial interest.

■ ACKNOWLEDGMENTS

All authors appreciate the support from the National Science Foundation of China (No. 51506046) and the Program for Young Backbone Teachers in Colleges and Universities in Henan Province (No. 2018GGJS046).

■ REFERENCES

(1) Goulet, M. A.; Kjeang, E. Co-laminar Flow Cells for Electrochemical Energy Conversion. *J. Power Sources* **2014**, *260*, 186−196.

(2) Nasharudin, M. N.; Kamarudin, S. K.; Hasran, U. A.; Masdar, M. S. Mass Transfer and Performance of Membrane-less Micro Fuel Cell: A Review. *Int. J. Hydrogen Energy* **2014**, *39*, 1039−1055.

(3) Zhao, T. S.; Chen, R.; Yang, W. W.; Xu, C. Small Direct Methanol Fuel Cells with Passive Supply of Reactants. *J. Power Sources* **2009**, *191*, 185−202.

(4) Zhou, X. L.; Zeng, Y. K.; Zhu, X. B.; Wei, L.; Zhao, T. S. A High-Performance Dual-Scale Porous Electrode for Vanadium Redox Flow Batteries. *J. Power Sources* **2016**, *325*, 329−336.

(5) Shang, M. G.; Zhang, J.; Liu, X. C.; Liu, Y.; Guo, S. P.; Yu, S. M.; Filatov, S.; Yi, X. B. N. S Self-Doped Hollow-Sphere Porous Carbon Derived from Puffball Spores for High Performance Supercapacitors. *Appl. Surf. Sci.* **2021**, *542*, No. 148697.

(6) Lei, W. D.; Yang, B. K.; Sun, Y. J.; Xiao, L. W.; Tang, D. Y.; Chen, K.; Sun, J.; Ke, J.; Zhuang, Y. Self-Sacrificial Template Synthesis of Heteroatom Doped Porous Biochar for Enhanced Electrochemical Energy Storage. *J. Power Sources* **2021**, *488*, No. 229455.

(7) Ott, S.; Orfanidi, A.; Schmies, H.; Anke, B.; Nong, H. N.; Hübner, J.; Gernert, U.; Gliech, M.; Lerch, M.; Strasser, P. Ionomer Distribution Control in Porous Carbon Supported Catalyst Layers for High Power and Low Pt-loaded Proton Exchange Membrane Fuel Cells. *Nat. Mater.* **2020**, *19*, 77−85.

(8) Weerathunga, D. T. D.; Jayawickrama, S. M.; Phua, Y. K.; Nobori, K.; Fujigaya, T. Effect of Polytetrafluoroethylene Particles in Cathode Catalyst Layer Based on Carbon Nanotube for Polymer Electrolyte Membrane Fuel Cells. *Bull. Chem. Soc. Jpn.* **2019**, *92*, 2038−2042.

(9) Zou, X.; Wang, L.; Yakobson, B. Mechanisms of the Oxygen Reduction Reaction on B- and/or N-doped Carbon nanomaterial with curvature and edge effects. *Nanoscale* **2018**, *10*, 1129−1134.

(10) Qian, Y.; An, T.; Sarnello, E.; Liu, Z.; Li, T.; Zhao, D. Janus Electrocatalysts Containing MOF-Derived Carbon Networks and NiFe-LDH Nanoplates for Rechargeable Zinc-Air Batteries. *ACS Appl. Energy Mater.* **2019**, *2*, 1784−1792.

(11) Zhang, C. L.; Lu, B. R.; Cao, F. H.; Wu, Z. Y.; Zhang, W.; Cong, H. P.; Yu, S. H. Electrospun Metal-Organic Framework Nanoparticle Fibers and Their Derived Electrocatalyst for Oxygen Reduction Reaction. *Nano Energy* **2019**, *55*, 226−233.

(12) Wang, J.; Kong, H.; Zhang, J. Y.; Hao, Y.; Shao, Z. P.; Ciucci, F. Carbon-based Electrocatalysts for Sustainable Energy Applications. *Prog. Mater. Sci.* **2021**, *116*, No. 100717.

(13) Wang, R.; Li, Y. S. Carbon Electrodes Improving Electrochemical Activity and Enhancing Mass and Charge Transports in Aqueous Flow Battery: Status and Perspective. *Energy Storage Mater.* **2020**, *31*, 230−251.

(14) Li, Y. M.; Pu, Z. Y.; Sun, Q. M.; Pan, N. A Review on Novel Activation Strategy on Carbonaceous Materials with Special Morphology/Texture for Electrochemical Storage. *J. Energy Chem.* **2021**, *60*, 572−590.

(15) Sorokin, A. E.; Petrova, G. N.; Donskikh, I. N. Use of Chemical and Electrochemical Treatment Methods in the Liquid-Phase Modification of Carbon Fiber and Fiberglass Surfaces in the Production of Construction Materials: A Review. *Theor. Found. Chem. Eng.* **2020**, *54*, 1061−1067.

(16) Labaran, B. A.; Vohra, M. S. Application of Activated Carbon Produced from Phosphoric Acid-based Chemical Activation of Oil Fly Ash for the Removal of some Charged Aqueous Phase Dyes: Role of Surface Charge, Adsorption Kinetics, and Modeling. *Desalin. Water Treat.* **2016**, *57*, 16034−16052.

(17) Zamouche, M.; Arris, S.; LeHocine, M. B. Removal of Rhodamine B from Water by Cedar Cone: Effect of Calcinations and Chemical Activation. *Int. J. Hydrogen Energy* **2014**, *39*, 1523−1531.

(18) Nandhini, R.; Mini, P. A.; Avinash, B.; Nair, S. V.; Subramanian, K. R. V. Supercapacitor Electrodes Using Nanoscale

Activated Carbon from Graphite by Ball Milling. *Mater. Lett.* **2012**, *87*, 165−168.
(19) Raymundo-Piñero, E.; Azaïs, P.; Cacciaguerra, T.; Cazorla-Amorós, D.; Linares-Solano, A.; Béguin, F. KOH and NaOH Activation Mechanisms of Multiwalled Carbon Nanotubes with Different Structural Organisation. *Carbon* **2005**, *43*, 786−795.
(20) Zhang, S.; Xi, J. Y.; Zhou, H. P.; Qiu, X. P.; et al. KOH Etched Graphite Felt with Improved Wettability and Activity for Vanadium Flow Batteries. *Electrochim. Acta* **2016**, *206*, 36−43.
(21) Ishifune, M.; Suzuki, R.; Mima, Y.; Uchida, K.; Yamashita, N.; Kashimura, S. Novel Electrochemical Surface Modification Method of Carbon Fiber and its Utilization to the Preparation of Functional Electrode. *Electrochim. Acta* **2005**, *51*, 14−22.
(22) Deng, J.; Xiong, T. Y.; Xu, F.; Li, M. M.; Han, C. L.; Gong, Y. T.; Wang, H. Y.; Wang, Y. Inspired by Bread Leavening: One-pot Synthesis of Hierarchically Porous Carbon for Supercapacitors. *Green Chem.* **2015**, *17*, 4053−4060.
(23) Xu, H.; Zhang, H.; Wang, H.; Leung, D. Y.; Zhang, L.; Cao, J.; Jiao, K.; Xuan, J. Counter-Flow Formic Acid Microfluidic Fuel Cell with High Fuel Utilization Exceeding 90%. *Appl. Energy* **2015**, *160*, 930−936.
(24) Li, D.; Xu, H.; Zhang, L.; Leung, D. Y. C.; Vilela, F.; Wang, H.; Xuan, J. Boosting the Performance of Formic Acid Microfluidic Fuel Cell: Oxygen Annealing Enhanced Pd@graphene Electrocatalyst. *Int. J. Hydrogen Energy* **2016**, *41*, 10249−10254.
(25) Kjeang, E.; Brolo, A. G.; Harrington, D. A.; Djilali, N.; Sinton, D. Hydrogen Peroxide as an Oxidant for Microfluidic Fuel Cells. *J. Electrochem. Soc.* **2007**, *154*, B1220−B1226.
(26) Kjeang, E.; Michel, R.; Harrington, D. A.; Sinton, D.; Djilali, N. An Alkaline Microfluidic Fuel Cell Based on Formate and Hypochlorite Bleach. *Electrochim. Acta* **2008**, *54*, 698−705.
(27) López-Montesinos, P. O.; Yossakda, N.; Schmidt, A.; Brushett, F. R.; Pelton, W. E.; Kenis, P. J. A. Design, Fabrication, and Characterization of a Planar, Silicon-based, Monolithically Integrated Micro Laminar Flow Fuel Cell with a Bridge-Shaped Microchannel Cross-section. *J. Power Sources* **2011**, *196*, 4638−4645.
(28) Salloum, K. S.; Hayes, J. R.; Friesen, C. A.; Posner, J. D. Sequential flow membraneless microfluidic fuel cell with porous electrodes. *J. Power Sources* **2008**, *180*, 243−252.
(29) Liu, C. M.; Liao, Q.; Zhu, X.; Yang, Y. Investigating the Composition of Iron Salts on the Performance of Microfluidic Fuel Cells. *Ind. Eng. Chem. Res.* **2018**, *57*, 1756−1762.
(30) Liu, C. M.; Liu, L.; Wang, X. T.; Xu, B.; Lan, W. J. Enhancing the Performance of Microfluidic Fuel Cells by Modifying the Carbon-Fiber Paper Cathode by Air Annealing and Acid Oxidation. *Ind. Eng. Chem. Res.* **2018**, *57*, 13557−13565.
(31) Anson, F. C. Exchange Current Densities for Fe(II)-Fe(III) Solutions in Sulfuric Acid and Perchloric Acid. *Anal. Chem.* **1961**, *33*, 939−942.
(32) Whalen, J. J., III; Weiland, J. D.; Searson, P. C. Electrochemical Deposition of Platinum from Aqueous Ammonium Hexachloroplatinate Solution. *J. Electrochem. Soc.* **2005**, *152*, C738−C743.
(33) Zhang, B.; Ye, D. D.; Li, J.; Zhu, X.; Liao, Q. Electrodeposition of Pd Catalyst Layer on Graphite Rod Electrodes for Direct Formic Acid Oxidation. *J. Power Sources* **2012**, *214*, 277−284.
(34) Kim, Y. J.; Lee, H. J.; Lee, S. W.; Cho, B. W.; Park, C. R. Effects of Sulfuric Acid Treatment on the Microstructure and Electrochemical Performance of a Polyacrylonitrile (PAN)-based Carbon Anode. *Carbon* **2005**, *43*, 163−169.
(35) Datsyuk, V.; Kalyva, M.; Papagelis, K.; Parthenios, J.; Tasis, D.; Siokou, A.; Kallitsis, I.; Galiotis, C. Chemical Oxidation of Multiwalled Carbon Nanotubes. *Carbon* **2008**, *46*, 833−840.
(36) Raghuveer, M. S.; Agrawal, S.; Bishop, N.; Ramanath, G. Microwave-assisted Single-step Functionalization and in situ Derivatization of Carbon Nanotubes with Gold Nanoparticles. *Chem. Mater.* **2006**, *18*, 1390−1393.
(37) Yue, L.; Li, W. S.; Sun, F. Q.; Zhao, L. Z.; Xing, L. D. Highly Hydroxylated Carbon Fibers as Electrode Materials of All-Vanadium Redox Flow Battery. *Carbon* **2010**, *48*, 3079−3090.
(38) Yang, D.; Guo, G. Q.; Hu, J. H.; Wang, C. C.; Jiang, D. L. Hydrothermal Treatment to Prepare Hydroxyl Group Modified Multi-walled Carbon Nanotubes. *J. Mater. Chem.* **2008**, *18*, 350−354.
(39) Kang, Z. H.; Wang, E. B.; Mao, B. D.; Su, Z. M.; Gao, L.; Niu, L.; Shan, H. Y.; Xu, L. Heterogeneous Hydroxylation Catalyzed by Multi-walled Carbon Nanotubes at Low Temperature. *Appl. Catal., A* **2006**, *299*, 212−217.
(40) Yang, W. Q.; Yang, S. H.; Sun, W.; Sun, G. Q.; Xin, Q. Nanostructured Silver Catalyzed Nickel Foam Cathode for an Aluminum-Hydrogen Peroxide Fuel Cell. *J. Power Sources* **2006**, *160*, 1420−1424.
(41) Sun, D.; Xue, X.; Tang, Y. G.; Jing, Y.; Huang, B.; Ren, Y.; Yao, Y.; Wang, H. Y.; Cao, G. Z. High Rate $LiTi_2(PO_4)_3$@N-C Composite via Bi-nitrogen Sources Doping. *ACS Appl. Mater. Interfaces* **2015**, *7*, 28337−28345.
(42) McDermott, C. A.; Kneten, K. R.; McCreery, R. L. Electron Transfer Kinetics of Aquated $Fe^{+3/+2}$, $Eu^{+3/+2}$, and $V^{+3/+2}$ at Carbon Electrodes. *J. Electrochem. Soc.* **1993**, *140*, 2593−2599.
(43) Chen, P. H.; Fryling, M. A.; McCreery, R. L. Electron Transfer Kinetics at Modified Carbon Electrode Surfaces: The Role of Specific Surface Sites. *Anal. Chem.* **1995**, *67*, 3115−3122.
(44) Yang, Y.; Liu, T. Y.; Zhu, X.; Zhang, F.; Ye, D. D.; Liao, Q.; Li, Y. Boosting Power Density of Microbial Fuel Cells with 3D Nitrogen-doped Graphene Aerogel Electrode. *Adv. Sci.* **2016**, *3*, No. 1600097.
(45) Qiu, W. D.; Xiao, H. B.; Yu, M. H.; Yu, L.; Lu, X. H. Surface Modulation of $NiCo_2O_4$ Nanowire Arrays with Significantly Enhanced Reactivity for Ultrahigh Energy Supercapacitors. *Chem. Eng. J.* **2018**, *352*, 996−1003.
(46) Yao, C.; Zhang, H.; Liu, T.; Li, X.; Liu, Z. Carbon Paper Coated with Supported Tungsten Trioxide as Novel Electrode for All-vanadium Flow Battery. *J. Power Sources* **2012**, *218*, 455−461.
(47) Lu, X. H.; Zeng, Y. X.; Yu, M. H.; Zhai, T.; Liang, C. L.; Xie, S. L.; Balogun, M. S.; Tong, Y. X. Oxygen Deficient Hematite Nanorods as High-Performance and Novel Negative Electrodes for Flexible Asymmetric Supercapacitors. *Adv. Mater.* **2014**, *26*, 3148−3155.
(48) Yang, Y.; Dong, R. Z.; Zhu, Y. L.; Li, H. S.; Zhang, H.; Fan, X. M.; Chang, H. L. High-performance Direct Hydrogen Peroxide Fuel Cells (DHPFCs) with Silver Nanowire-graphene Hybrid Aerogel as Highly-conductive Mesoporous Electrodes. *Chem. Eng. J.* **2020**, *381*, No. 122749.
(49) Lan, Q.; Ye, D. D.; Zhu, X.; Chen, R.; Liao, Q.; Zhang, T.; Zhou, Y. Direct Formate/Persulfate Microfluidic Fuel Cell with a Catalyst-Free Cathode and High Power Density. *ACS Sustainable Chem. Eng.* **2021**, *9*, 5623−5630.
(50) Hawthorne, K. L.; Wainright, J. S.; Savinell, R. F. Studies of Iron-Ligand Complexes for an All-Iron Flow Battery Application. *J. Electrochem. Soc.* **2014**, *161*, A1662−A1671.
(51) Gong, K.; Xu, F.; Grunewald, J. B.; Ma, X. Y.; Zhao, Y.; Gu, S.; Yan, Y. S. All-Soluble All-Iron Aqueous Redox-Flow Battery. *ACS Energy Lett.* **2016**, *1*, 89−93.
(52) Zhang, T.; Yu, C. H.; Zhu, X.; Ye, D. D.; Yang, Y.; Chen, R.; Liao, Q. Reduction of Formate Crossover in Sequential-Flow Microfluidic Fuel Cells. *Ind. Eng. Chem. Res.* **2021**, *60*, 1526−1531.

https://doi.org/10.1021/acsomega.1c02507
ACS Omega 2021, 6, 19153−19161